ARTICLE

Formation Mechanism of Biomass Aromatic Hydrocarbon Tar on Quantum Chemistry

Bo Chen[1], Bo Liu[2,*], Yong Chao[3] and Chao Zhong[1]

[1]School of Mechanical Engineering, Hunan Institute of Engineering, Xiangtan, 411104, China

[2]School of Electrical and Information Engineering, Hunan Institute of Engineering, Xiangtan, 411104, China

[3]Hunan Shuanghuan Fiber Forming Equipment Co., Ltd., Xiangtan, 411100, China

[*]Corresponding Author: Bo Liu. Email: liubo@hnie.edu.cn

ABSTRACT

The formation process of aromatic hydrocarbon tar during the pyrolysis process of biomass components of cellulose and lignin was carried out by quantum chemical calculation based on density functional theory method B3LYP/6-31G++(d, p). 5-Hydroxymethylfurfural was chosen as the model compound of cellulose and hemicellulose, and syringaldehyde was chosen as the model compound of lignin. The calculation results show that the formation process of cellulose monocyclic aromatic hydrocarbon tar is the conversion process of benzene ring from furan ring, and the highest reaction energy barrier appears in the process of decarbonylation, which is 370.8 kJ/mol. The formation of lignin monocyclic aromatic hydrocarbon tar is mainly the process of side chains removal and the formation of phenol, The highest reaction energy barrier appears in the process of decarbonylation, which is 374.9 kJ/mol. The reaction mechanism of phenanthrene formation from naphthalene was selected as the formation of cellulose and lignin polycyclic aromatic hydrocarbon tar. The calculation results show that he total barrier of the pathway that naphthalene dehydrogenates to form naphthalene free radicals and then reacts with ethylene twice by addition action, finally occurs cyclization reactions and isomerizes to produce phenanthrene is lowest, that is 38.6 kJ/mol. So it is proved that the evolution of tar is the process of deoxygenation and cyclization with the increase of the temperature from a theoretical point of view.

KEYWORDS

Cellulose; lignin; tar; aromatic hydrocarbon; quantum chemistry

1 Introduction

Guided by the goals of "Carbon peaking by 2030 and carbon neutrality by 2060", biomass energy is getting more and more attention [1]. The focus and difficulty of biomass energy utilization lie in the treatment of tar [2]. The definition of biomass tar is an important issue in the research of tar. A clear definition of biomass tar was attempted to give by scholars at home and abroad [3]. Biomass tar was defined as a condensable organic pollutant whose chemical components are mainly monocyclic and polycyclic aromatic compounds (PAHs), with a molecular weight greater than benzene [4]. A broader definition of tar was given by Milne et al. [5] of National Renewable Energy Laboratory (NREL) in the United States, which is that all the organic compounds of aromatic hydrocarbon with larger molecular

weight produced under pyrolysis and gasification can be regarded as tar. Based on Milne's research, Dayton [6] believed that the condensable produced in the process of pyrolysis and gasification is tar, and its chemical components are macromolecular aromatic hydrocarbons, including benzene. However, Moersch thought that benzene was used as the dividing substance of tar need to be discussed. Furthermore, whether it will block and corrode the equipment should be the standard to define tar [7]. The chemical composition of tar is complex, and these compounds have different dew-points. Up to now, tar still has not been given a unified definition. The reasons lie in its complicated components. As the conditions of biomass pyrolysis and gasification change, the chemical composition of tar produced changes as well. The analysis of tar has to be based on specific experimental conditions. The classification is also hard to be defined [8]. In summary, the major classifications are based on the composition of tar, the dew point of tar, the location of tar production, and the characteristics of tar. Tar was divided into primary, secondary and tertiary tar on the basis of the three components of biomass by Evans of NREL [9]. Elliott holds that the temperature of generation determines the composition of tar. In the light of temperature, tar is classified into oxygenated mixture, phenol hexyl ether, alkylphenol, heterocyclic ether, PAH and PAH with higher molecular weight [10]. According to the composition of organic compounds in tar, Tar was divided into four groups by Hasler, which is that the sum of high molecular weight organic compounds, PAH, aromatic compounds containing one or more phenolic hydroxyls and water soluble organic matter residue [11]. Tar was divided into two major categories based on the reactivity of tar by Perez et al. [12] and Corella et al. [13], that is, "easy to break" tar with good reactivity and "hard to break" with poor reactivity. Although scholars came to different research conclusions and hold different opinions on the definition and classification of tar, it is difficult to understand tar thoroughly from the location, characteristics and dew point of tar production. The composition of tar changes when temperature rises, which reflects the formation process of tar to a certain extent. Generally, it is the process of deoxidation and cyclization. The formation process of aromatic tar can be regarded as the main line of tar formation.

The mechanism of thermal cracking of biomass components has been studied by scholars. The cracking process of D-glucopyranose monomer was calculated and deduced by Wang et al. [14]. The study concluded that D-glucopyranose undergoes four transition states and finally generated 5-hydroxymethyl base furfural, which further generates furfural. Through the analysis of the reaction energy barrier, the opening of the glucose ring is relatively easy, and the cyclization to furan is relatively difficult. The xylan cycle unit was used as a model to simulate the formation mechanism of furfural by Zhang et al. [15]. The study concluded that highest reaction energy barrier of xylan to furfural was calculated to be 236 kJ/mol. Eugenol was used as a lignin model for pyrolysis analysis, which formed 3-methoxycatechol, 2-methoxy-6-methylphenol were carried out chemical calculations. The result shows that the total reaction energy barriers are 366.6, 474.8 kJ/mol [16]. In order to analyze the cracking mechanism of lignin, 1-guaiacol-2-(2-methoxybenzene) oxy)-1,3 propanediol was selected as the model. The results show that: 1-guaiacol-2-(2-methoxyphenoxy)-1,3-propanediol pyrolysis can generate guaiacol, 1-guaiacol-3-hydroxyacetone, 3-Guaiacyl-3-hydroxypropionaldehyde, guaiacyl formaldehyde, etc., the reaction energy barrier is in the range of 265~442 kJ/mol [17].

The main components of tar are aromatic compounds, so the formation and cracking mechanism of biomass aromatic hydrocarbon tar from the molecular level is need. In this paper, the formation mechanism of monocyclic aromatic hydrocarbon tars from biomass and the formation mechanism of three rings polycyclic aromatic hydrocarbon tars from three rings polycyclic aromatic hydrocarbon tars were researched.

2 The Formation Mechanism of Monocyclic Aromatic Hydrocarbon Tar

2.1 The Mechanism of Benzene Formation from 5-HMF

5-HMF is an important product of the pyrolysis of cellulose and hemicellulose. Its formation process has been extensively researched, and the decarboxylation, decarbonylation and cyclization reactions of further pyrolysis of 5-HMF was deduced through experiments [18]. However, there is lack of studies on the pyrolysis mechanism of 5-HMF. The reaction pathway in Fig. 1 is designed to show the process of pyrolysis of 5-HMF to benzene. The mechanism was studied by density functional theory B3LYP/6-31G ++(d, p) of Gaussian software. The standard thermodynamic parameters under pressure 1.13×105 Pa and temperature 298 K were obtained.
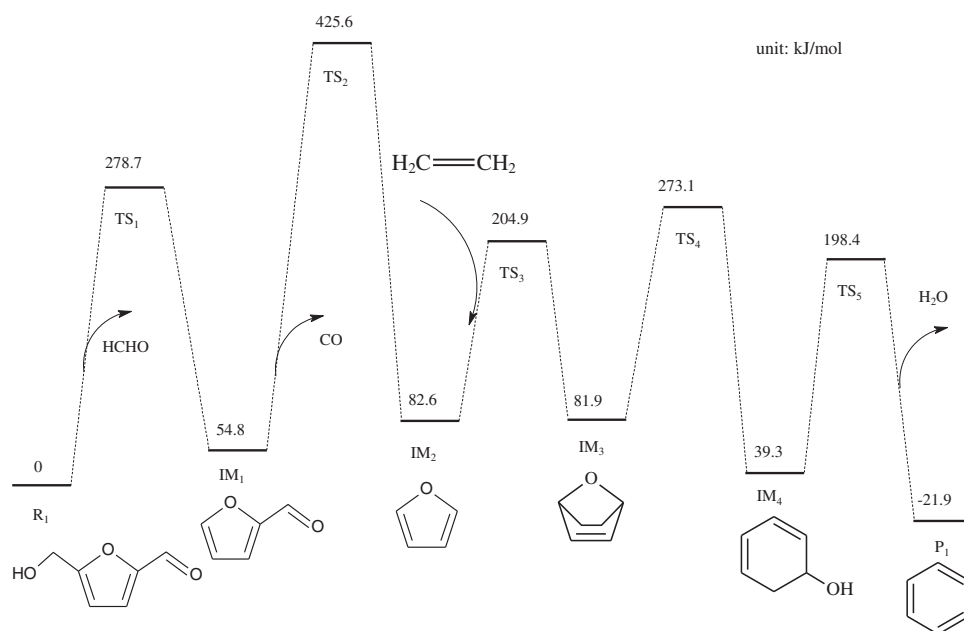
Figure 1: Proposed reaction pathway and energy profiles of benzene formation from pyrolysis of furfural
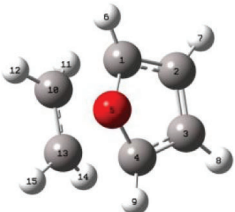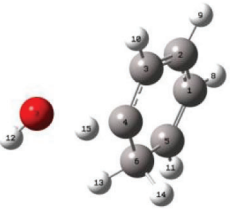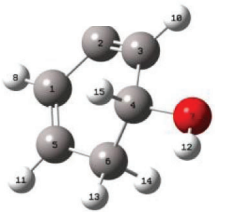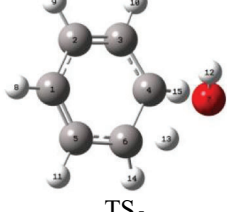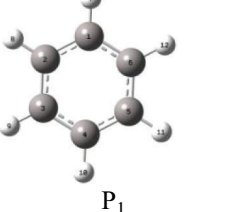
5-HMF first removes hydroxymethyl to form formaldehyde and furfural. Furfural removes formaldehyde side chains to form furan, which releases heat of 27.8 kJ/mol. The transition state is TS_2 and the reaction energy barrier is 370.8 kJ/mol. The furan reacts with ethylene to forms IM_3, which emits a small amount of heat of 0.6 kJ/mol. The transition state is TS_3 and the reaction energy barrier is 122.4 kJ/mol. IM_3 undergoes an isomerization reaction to form IM_4, which releases energy of 42.6 kJ/mol. TS_4 is the transition state and the reaction energy barrier is 191.2 kJ/mol. IM_4 undergoes dehydration reaction to form benzene, which emits heat of 92.2 kJ/mol. The transition state is TS_5 and the reaction energy barrier is 159.1 kJ/mol. The possibility of generating benzene from 5-HMF is theoretically verified, which is consistent with Yang Hao's speculation [18]. The reaction energy of furfural pyrolysis to benzene is shown in Fig. 1 in details. The optimized geometric configurations of reactants, products, intermediates and transition states in the reaction pathway are presented in Table 1.

2.2 The Mechanism of Phenol Formation from Syringaldehyde

The process of forming aromatic hydrocarbon tar from lignin was designed as follows: Phenolic substances forms from primary tar, and then phenolic substances are further converted into aromatic hydrocarbon substances. The pyrolysis process of phenols from structural units can be used as an

important means to analyse the formation of aromatic tars from lignin primary tars. Syringal is one of the representative substances of syringyl phenols. Its side chain is composed of hydroxyl group, aldehyde group and methoxy group so it is a typical syringyl phenol. Fig. 2 shows the chemical structural formula of syringaldehyde and the homolysis of ten kinds of molecular bonds. Table 2 is the calculation result of the dissociation energies of various major bonds. The order of dissociation energy of various bonds in syringaldehyde is $CH_3—O < O—H < CH_2—H < CH_3O—C_{aromatic} < HO—C_{aromatic} < C_{aromatic}—H$.

Table 1: Optimized structure of reactants, products, intermediates and transition states in reaction pathway of benzene formation from pyrolysis of furfural (unit: nm)

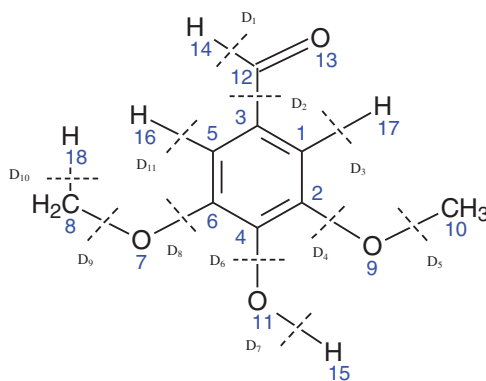| Species	Bond length	Species	Bond length	Species	Bond length
IM_4	R(1, 2) 1.42 R(1, 5) 1.38 R(1, 10) 2.14 R(4, 13) 2.14 R(4, 9) 1.08	IM_3	R(1, 2) 1.53 R(1, 5) 1.57 R(1, 7) 1.45 R(1, 8) 1.09 R(2, 3) 1.35	TS_4	R(1, 2) 1.44 R(1, 5) 1.36 R(4, 15) 1.25 R(4, 7) 2.42 R(7, 12) 0.97
TS_3	R(1, 2) 1.47 R(1, 5) 1.35 R(4, 7) 1.43 R(4, 6) 1.54 R(7, 12) 0.97	TS_5	R(1, 2) 1.43 R(1, 5) 1.37 R(4, 15) 1.08 R(7, 13) 1.41 R(7, 12) 0.97	P_1	R(1, 2) 1.40 R(1, 6) 1.40 R(1, 7) 1.09 R(2, 3) 1.40 R(2, 8) 1.09

Figure 2: Homolytic cleavage ways of syringaldehyde

Table 2: Bond dissociation energies (D) of the major bonds in syringaldehyde (unit: kJ/mol)

Bond B[C(12)—H(14)]	D_1 372.5	Bond B[C(3)—C(12)]	D_2 474.9	Bond B[C(1)—C(17)]	D_3 433.6
Bond B[C(2)—O(9)]	D_4 389.8	Bond B[O(9)—C(10)]	D_5 215.6	Bond B[C(4)—O(11)]	D_6 452.0
Bond B[O(11)—H(15)]	D_7 335.1	Bond B[C(6)—O(7)]	D_8 376.1	Bond B[O(7)—C(8)]	D_9 223.9
Bond B[C(8)—H(18)]	D_{10} 398.6	Bond B[C(5)—H(16)]	D_{11} 467.4		

Based on the results of the dissociation energy of the syringaldehyde bond and the quantum chemical analysis of the pyrolysis pathway of syringol [16], the pyrolysis reaction pathway of syringaldehyde is shown in Fig. 3. The density functional theory method B3LYP/6-31G++(d, p) is applied to carry out the quantum chemical theoretical research on the pyrolysis reaction mechanism of syringaldehyde The standard thermodynamic parameters under pressure 1.13×105 Pa and temperature 500 K were obtained. The reactants, products, intermediates and transition states of various reactions are fully optimized by the energy gradient technique. The Potential energy profiles of phenol formation from pyrolysis of syringaldehyde is shown in Fig. 4. A hydrogenation reaction occurring on the carbon atom adjacent to the benzene ring and the methoxy group forms IM_5, which releases heat of 121.1 kJ/mol. The transition state is TS_6 and the reaction energy barrier is 24.2 kJ/mol. This hydrogenation reaction reduces the stability of the benzene ring structure and facilitates the overall removal of methoxy groups. This indicates that for lignin monomers such as syringaldehyde, hydrogenation of carbon atoms adjacent to the methoxy group can reduce the reaction energy barrier of the demethoxy reaction. IM_5 removes the entire methoxy group to form IM_6, absorbing heat of 50.3 kJ/mol. The methyl group on the other side of IM_6 removes an H to form a free radical IM_7 which absorbs heat of 392.7 kJ/mol. Through the isomeric transformation, IM_7 forms the intermediate IM_8. A further isomeric reaction on IM_8 forms IM_9, which releases heat of 54.2 kJ/mol. The process transforming IM_9 into IM_{11} through IM_{10} is the process of changing the position of methylene and oxygen atoms. IM_9, going through the transition state TS8, undergoes dehydrogenation to form IM_{10}. This reaction absorbs heat of 65.8 kJ/mol and the energy barrier is 98.8 kJ/mol. IM_{10} undergoes decarbonylation to form IM_{11} with CO produced, which goes through the transition state TS_9 and the reaction absorbs heat of 12.9 kJ/mol, the reaction energy barrier is 349.2 kJ/mol. The decarbonylation of IM_{11} forms P_2 with CO produced, which goes through the transition state TS_{10} and the reaction absorbs heat 27.1 kJ/mol, the energy barrier is 374.9 kJ/mol. The decarbonylation of IM_{11} forms P_2 with CO produced. It shows that there are two pathways of methoxy removal. It shows that there are two ways to remove the methoxy group. One is that methoxy group forms a carbonyl group after isomerization of the methoxy group with the small molecule gas CO produced. The other is that the carbon atom adjacent of the methoxy group occurs hydrogenation reaction to destroy the stability of the benzene ring, and then the entire methoxy group is removed. Therefore, some experimental results of the pyrolysis of bio-oil to generate tar are theoretically verified: the molecular weight is getting smaller and smaller, and the generation of phenol is generated by the removal of side chains from various free radicals containing benzene rings [18]. The geometric structures of the reactants, transition states, intermediates and products are shown in Table 3.
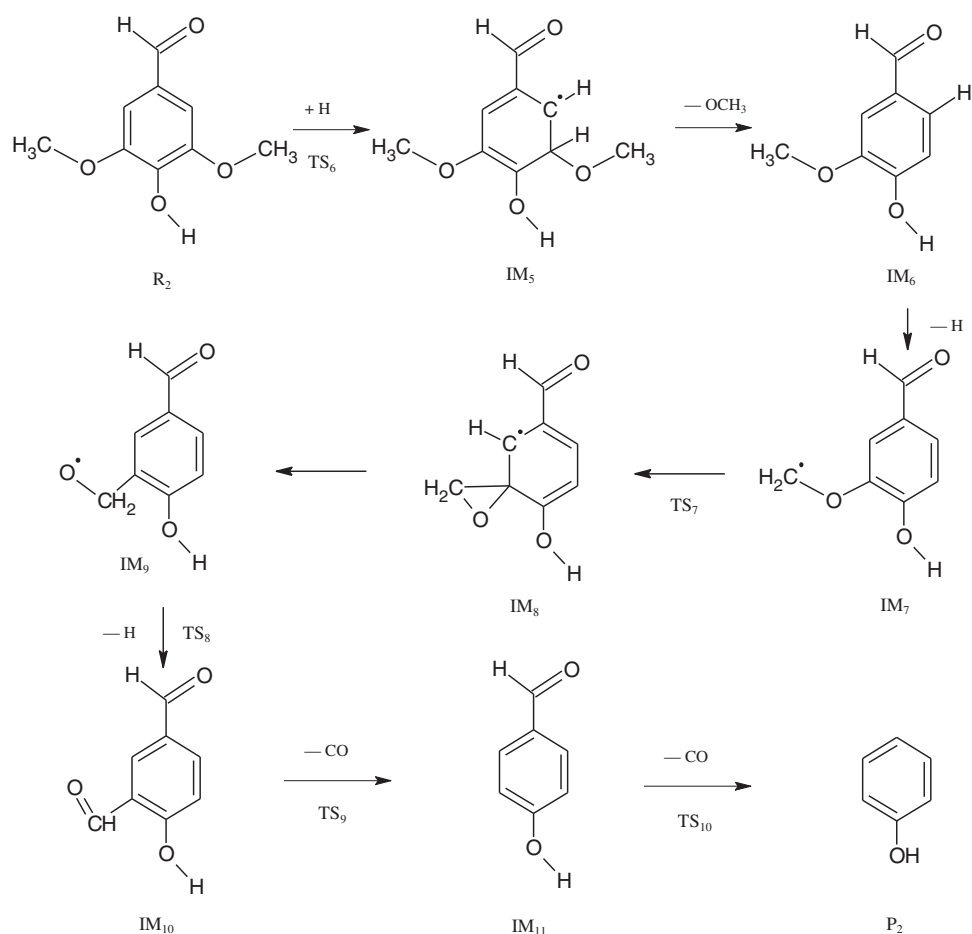
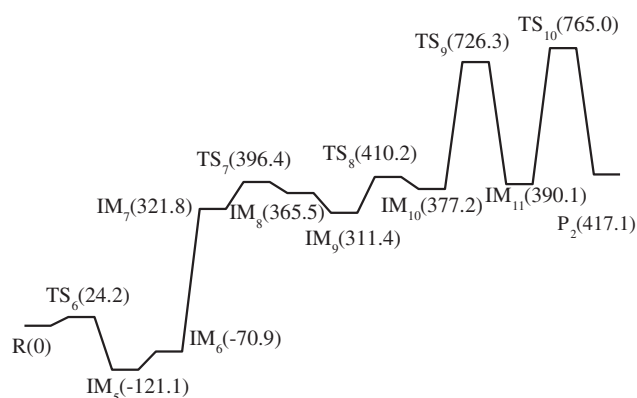**Figure 3:** Proposed reaction pathway of phenol formation from pyrolysis of syringaldehyde
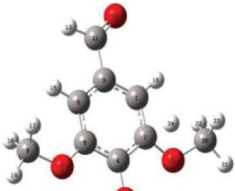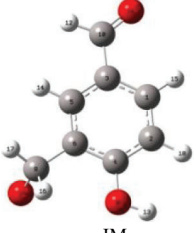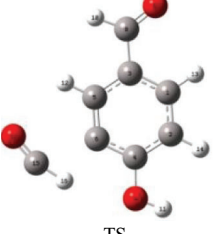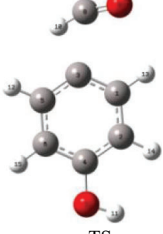

Figure 4: Potential energy profiles of phenol formation from pyrolysis of syringaldehyde

The formation of cellulose and lignin includes deoxygenation. High temperature promotes the breakage of the oxygen-containing functional groups. 5-HMF can be deoxygenated to form benzene rings, and the basic structural unit of lignin can also form phenols, which is consistent with the experimental results [19,20].

Table 3: Optimized structure of reactants, products, intermediates and transition states in reaction pathway of phenol formation from pyrolysis of syringaldehyde (unit: nm)

Species	Bond length	Species	Bond length	Species	Bond length
TS$_6$	R(1, 2) 1.410 R(3, 11) 1.476 R(6, 7) 1.361 R(2, 9) 1.377 R(4, 10) 1.347	IM$_5$	R(1, 2) 1.495 R(2, 9) 1.374 R(6, 7) 1.352 R(7, 8) 1.425 R(4, 11) 1.363	IM$_6$	R(1, 2) 1.392 R(4, 9) 1.361 R(6, 7) 1.361 R(3, 10) 1.474 R(10, 11) 1.221
IM$_7$	R(1, 2) 1.391 R(3, 10) 1.476 R(6, 7) 1.371 R(4, 9) 1.359 R(7, 8) 1.363	TS$_7$	R(1, 2) 1.389 R(3, 10) 1.476 R(4, 9) 1.356 R(7, 8) 1.364 R(6, 7) 1.416	IM$_8$	R(1, 2) 1.404 R(3, 10) 1.481 R(4, 9) 1.357 R(7, 8) 1.418 R(6, 7) 1.505
IM$_9$	R(1, 2) 1.388 R(3, 10) 1.475 R(4, 9) 1.363 R(6, 8) 1.514 R(7, 8) 1.376	TS$_8$	R(1, 2) 1.386 R(3, 10) 1.476 R(4, 9) 1.350 R(7, 8) 1.230 R(7, 16) 2.372	IM$_{10}$	R(1, 2) 1.386 R(4, 7) 1.360 R(6, 15) 1.483 R(15, 17) 1.221 R(3, 8) 1.478
TS$_9$	R(1, 2) 1.391 R(4, 7) 1.375 R(3, 8) 1.474 R(15, 16) 1.097 R(15, 17) 1.165	IM$_{11}$	R(1, 2) 1.397 R(3, 8) 2.086 R(8, 9) 1.173 R(8, 10) 1.097 R(4, 7) 1.371	TS$_{10}$	R(1, 2) 1.399 R(1, 7) 1.085 R(2, 12) 1.372 R(12, 13) 0.966 R(5, 6) 1.399

3 The Formation Process of Polycyclic Aromatic Hydrocarbons Tar

As the temperature of aromatic hydrocarbon tar increases, the degree of aromaticity strengthens. Naphthalene is the main component of aromatic tar containing two PAH benzene rings [21]. Li et al. [22] found that at 800°C, the proportion of bicyclic PAHs in tar is 55%, and the content of naphthalene in aromatic tar accounts for 30% at 800°C. Phenanthrene is the main component of aromatic tar containing three PAHs benzene rings. The proportion of tricyclic PAHs in tar is 20%, and the content of phenanthrene in the aromatic tar accounts for 20% at 800°C. Based on the relevant experiments of the process of naphthalene forming phenanthrene and the HACA (hydrogen abstraction-acetylene addition) studied by Kislov et al. [23], three reaction pathways of phenanthrene formation from naphthalene were designed as Figs. 5–7.
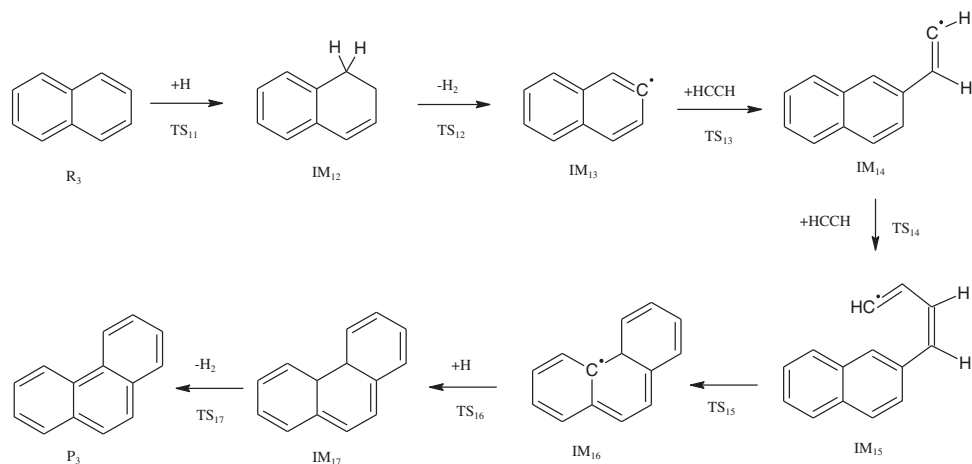
Figure 5: Proposed reaction pathway 1 of phenanthrene formation from pyrolysis of naphthalene
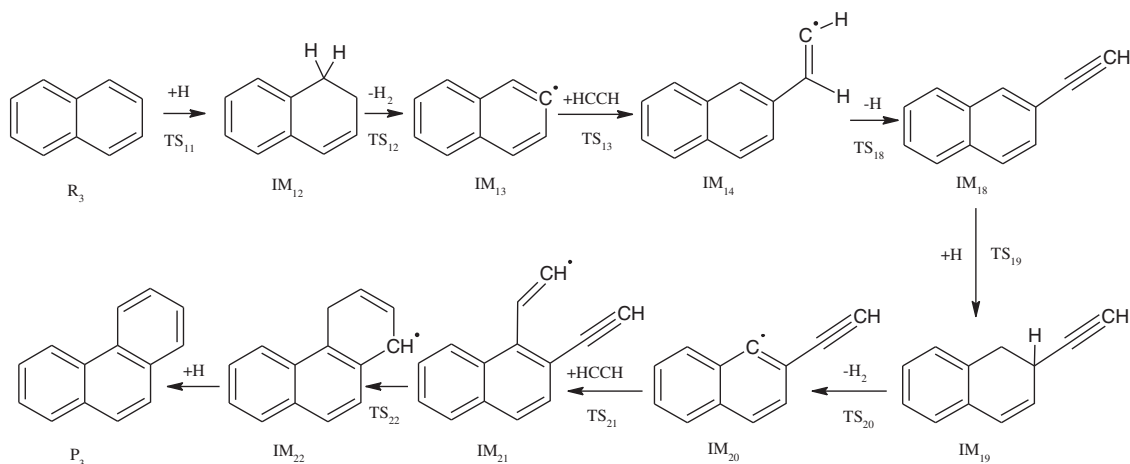

Figure 6: Proposed reaction pathway 2 of phenanthrene formation from pyrolysis of naphthalene

The density functional theory method B3LYP/6-31G ++(d, p) was adopted to conduct a quantum chemical theoretical study on the pyrolysis reaction mechanism of phenanthrene formation from biphenyl. The standard thermodynamic parameters under pressure 1.13×10^5 Pa and temperature 700 K were obtained. The reactants, products, intermediates and transition states of various reactions are fully optimized by the energy gradient technique. In the reaction pathway 1, phenanthrene formation from naphthalene, naphthalene undergoes hydrogenation reaction first to form IM_{12}, which releases heat of 133.6 kJ/mol. The transition state is TS_{11} and the reaction energy barrier is 3.8 kJ/mol. After the dehydrogenation, IM_{12} forms naphthalene radical IM_{13} and generates H_2, which emits heat of 133.0 kJ/mol. The transition state is TS_{12} and the reaction energy barrier is 172.2 kJ/mol. The addition reaction occurs between IM_{13} and acetylene to produces IM_{14}, which emits heat of 91.9 kJ/mol and passes through the transition state TS_{13} with a reaction energy barrier of 109.5 kJ/mol. IM_{14} continues to undergo the addition reaction with acetylene to form IM_{15}, which emits heat of 150.7 kJ/mol, and its reaction energy barrier is 23.2 kJ/mol. IM_{15}, a naphthalene radical, reacting with ethylene twice by addition action to form butadiene side chains, and the side chains gradually cyclizes to form phenanthrene radical IM_{16}, which emits heat of 157.3 kJ/mol. The reaction goes through the transition state TS_{15} and the reaction energy barrier is 7.1 kJ/mol. Hydrogenation reaction occurs on IM_{16} to

produce IM_{17} with the heat of 139.3 kJ/mol emitted, which goes through the transition state TS_{16} and the reaction energy barrier is 99.4 kJ/mol. Dehydrogenation reaction occurs on IM_{17} to form phenanthrene and generates H_2 with heat of 250.8 kJ/mol emitted, which goes through the transition state TS_{17} and the reaction energy barrier is 225.1 kJ/mol. The potential energy profiles of this reaction pathway is shown in Fig. 8.
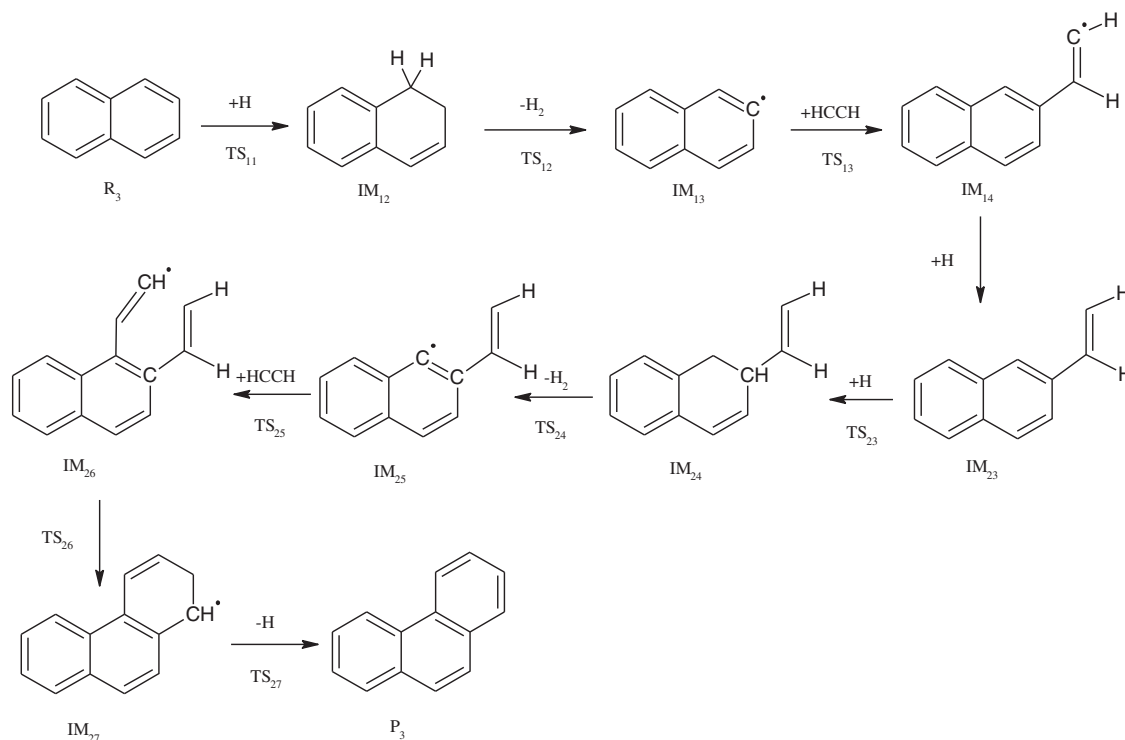

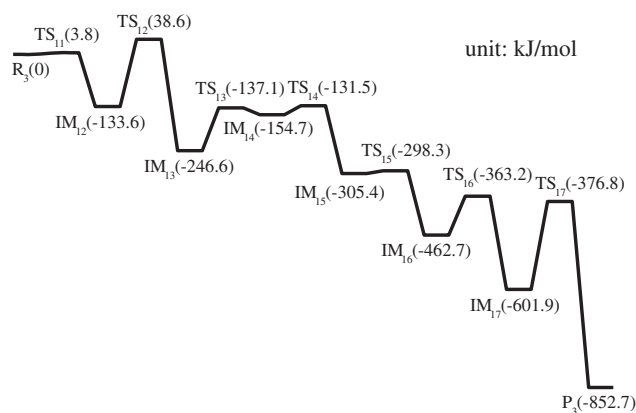**Figure 7:** Proposed reaction pathway 3 of phenanthrene formation from pyrolysis of naphthalene

Figure 8: Potential energy profiles of reaction pathway 1 of phenanthrene formation from pyrolysis of naphthalene

As for the reaction pathway 2 of phenanthrene from naphthalene, the kinetic process of naphthalene to intermediate IM_{14} is the same as that of reaction pathway 1. Then, the dehydrogenation reaction of IM_{14} side

chain makes the vinyl side chain convert to ethynyl, and finally form the intermediate IM_{18}. The reaction absorbs heat of 157.6 kJ/mol, which goes through the transition state TS_8 and the reaction energy barrier is 169.8 kJ/mol. The hydrogenation reaction can destroy the stability of the benzene ring structure and reduce the reaction energy barrier for the subsequent formation of free radicals. IM_{19} forms the intermediate IM_{20} with H_2 produced through the dehydrogenation reaction and the reaction absorbs heat of 105.1 kJ/mol, which goes through the transition state TS_{20} and the reaction energy barrier is 128.5 kJ/mol. IM_{20} continues to react with acetylene to form IM_{21}. The difference from reaction pathway 1 is that the acetylene does not react with the ethynyl group on the original side chain, but carries out the addiction reaction on the benzene ring to generate another vinyl side chain. The addition reaction is an endothermic reaction, which absorbs heat of 154.1 kJ/mol. The transition state TS_{21} and the reaction energy barrier is 15.6 kJ/mol. The acetylene and vinyl side chains on IM_{21} are cyclized to form phenanthrene radical IM_{22}, which absorbs heat of 259.0 kJ/mol. The transition state TS_{22} and the reaction energy barrier is 11.6 kJ/mol. The phenanthrene free radical IM_{22} generates phenanthrene after hydrogenation, and the reaction emits heat of 463.8 kJ/mol. The potential energy profile of the reaction path is shown in Fig. 9.
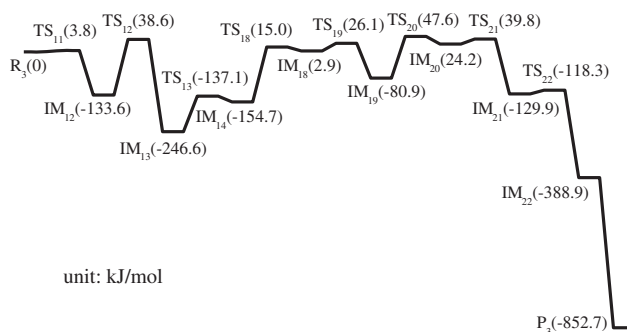

Figure 9: Potential energy profiles of reaction pathway 2 of phenanthrene formation from pyrolysis of naphthalene

In reaction pathway 3 of phenanthrene formation from naphthalene, the kinetic process of naphthalene to intermediate IM_{14} is the same as that of reaction pathways 1 and 2. And then the carbon atoms at the end of IM_{14} side chain undergoes the hydrogenation reaction to form the intermediate IM_{23}, which emits 456.2 kJ/mol of heat. IM_{23} proceeds with the hydrogenation reaction to form intermediate IM_{24}. The position of hydrogenation is the carbon atom connected to the benzene ring and the side chain. The hydrogenation reaction is an exothermic reaction, emitting heat of 88.3 kJ/mol. This reaction passes through the transition state TS_{23} and the reaction energy barrier is 18.3 kJ/mol. The structural stability of the benzene ring after hydrogenation is less stable, which reduces the reaction energy barrier for the formation of subsequent free radicals. The dehydrogenation reaction of IM_{24} produces the intermediate IM_{25} with heat of 102.1 kJ/mol absorbed. The reaction passes through the transition state TS_{24} and the reaction energy barrier is 106.6 kJ/mol. The addition reaction between IM_{25} and acetylene produces IM_{26}, which absorbs heat of 134.4 kJ/mol. The reaction passes through the transition state TS_{25}, and the reaction energy barrier is 26.5 kJ/mol. After this reaction, the two side chains of IM_{26} form a bond to form IM_{27} with an exotherm of 229.2 kJ/mol, which goes through the transition state TS_{26} and the reaction energy barrier is 1.0 kJ/mol. Finally, the dehydrogenation of IM_{27} produces phenanthrene, which is an exothermic reaction with heat absorption of 108.1 kJ/mol. The reaction goes through the transition state TS_{27}, the reaction energy barrier is 115.3 kJ/mol. The potential energy profile of this reaction pathway is shown in Fig. 10. The geometric structures of the reactants, transition states, intermediates and products are shown in Table 4.
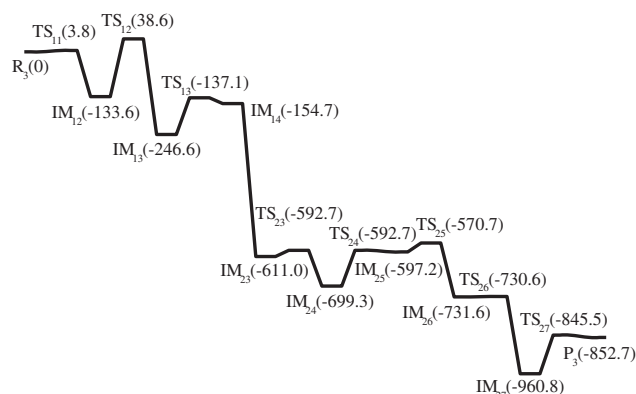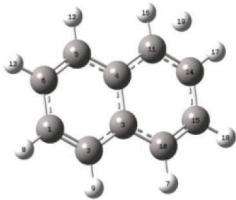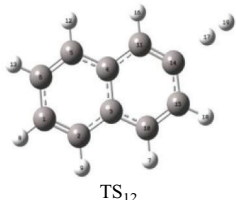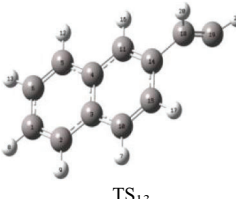
Figure 10: Potential energy profiles of reaction pathway 3 of phenanthrene formation from pyrolysis of naphthalen

Table 4: Optimized structure of reactants, products, intermediates and transition states in reaction pathway of phenanthrene formation from pyrolysis of naphthalene (unit: nm)
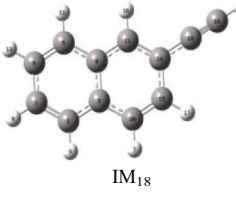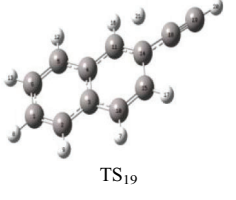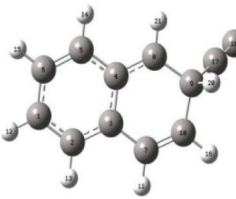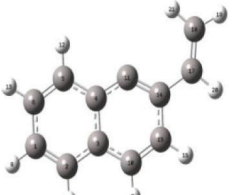
Species	Bond length	Species	Bond length	Species	Bond length
TS₁₁	R(1, 2) 1.379 R(2, 3) 1.422 R(3, 4) 1.432 R(11, 19) 1.991 R(11, 14) 1.392	IM₁₂	R(1, 2) 1.389 R(2, 3) 1.415 R(3, 4) 1.422 R(11, 19) 1.104 R(11, 14) 1.500	TS₁₂	R(1, 2) 1.378 R(2, 3) 1.423 R(11, 14) 1.364 R(14, 17) 1.500 R(17, 19) 0.848
TS₁₃	R(1, 2) 1.378 R(14, 18) 1.498 R(18, 19) 1.315 R(18, 20) 1.100 R(19, 21) 1.082	IM₁₄	R(1, 2) 1.378 R(14, 18) 1.476 R(18, 19) 1.321 R(18, 20) 1.098 R(19, 21) 1.081	TS₁₅	R(9, 11) 1.488 R(11, 13) 1.347 R(13, 14) 1.471 R(14, 15) 1.324 R(15, 24) 1.082
TS₁₈	R(14, 18) 1.442 R(18, 19) 1.225 R(19, 21) 1.067 R(18, 20) 1.958 R(19, 20) 2.458	IM₁₈	R(14, 18) 1.430 R(18, 19) 1.213 R(19, 20) 1.066 R(11, 16) 1.086 R(15, 17) 1.085	TS₁₉	R(14, 18) 1.440 R(18, 19) 1.211 R(19, 20) 1.066 R(14, 21) 1.805 R(14, 15) 1.448
IM₁₉	R(8, 9) 1.510 R(9, 10) 1.517 R(9, 20) 1.109 R(9, 17) 1.477 R(17, 18) 1.210	TS₂₀	R(14, 18) 1.429 R(18, 19) 1.212 R(19, 20) 1.066 R(11, 16) 1.513 R(16, 21) 0.843	TS₂₁	R(1, 2) 1.392 R(4, 9) 1.361 R(6, 7) 1.361 R(3, 10) 1.474 R(10, 11) 1.221
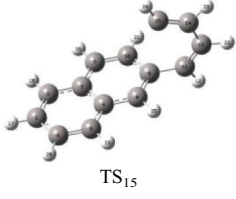
(Continued)

Table 4 (continued)

Species	Bond length	Species	Bond length	Species	Bond length
TS$_{23}$	R(1, 2) 1.391 R(3, 10) 1.476 R(6, 7) 1.371 R(4, 9) 1.359 R(7, 8) 1.363	IM$_{24}$	R(1, 2) 1.397 R(14, 17) 1.528 R(17, 18) 1.335 R(14, 23) 1.110 R(18, 21) 1.086	TS$_{24}$	R(1, 2) 1.382 R(14, 18) 1.485 R(18, 19) 1.339 R(14, 23) 2.369 R(19, 22) 1.836
IM$_{25}$	R(1, 2) 1.379 R(14, 17) 1.470 R(17, 18) 1.341 R(11, 14) 1.370 R(18, 21) 1.087	TS$_{26}$	R(11, 22) 1.477 R(22, 24) 1.327 R(13, 16) 1.465 R(16, 17) 1.351 R(17, 18) 1.086	TS$_{27}$	R(11, 13) 1.396 R(11, 12) 1.087 R(13, 22) 1.085 R(13, 25) 1.908 R(14, 15) 1.378

Three pathways were designed for the process of the formation of phenanthrene from naphthalene. The total energy barrier of reaction pathway 1 and reaction pathway 3 is 38.6 kJ/mol, which is slightly lower than 47.4 kJ/mol of reaction pathway 2, indicating that reaction pathways 1 and 3 are most likely to happen. By comparing the reaction energy barrier of the second addition reaction of acetylene in the three reaction pathways, pathway 1 is 23.2 kJ/mol, pathway 2 is 15.6 kJ/mol, and pathway 3 is 26.5 kJ/mol. So the reaction energy barrier of pathway 2 is the lowest. This shows that on the one hand, the way of the second addition action exerts some influence on the reaction energy barrier, and the energy barrier of addition reaction directly on the side chain is slightly smaller than that on the benzene ring adjacent to the original side chain. On the other hand, for the addition reaction happens at the adjacent position of the original side chain on the benzene ring, different functional groups of the original chain also affect the reaction energy barrier, and the ethynyl is more prone to acetylene addition than the carbon atom next to vinyl.

As the temperature further increased, the number of PAH rings in the tar increased, which further verified the experimental results [24,25]: 3-ring PAHs are generated from 2 rings at 500 K, and the temperature further increased, and 4-ring PAHs are slowly generated.

4 Conclusions

It is theoretically proved that the formation process of tar in the biomass pyrolysis process is the process of benzene cyclization, and the reaction path and reaction energy barrier are theoretically calculated. The difference between cellulose and lignin to form tar is that cellulose is a process of deoxygenation and remodeling cyclization, and the highest reaction energy barrier appears in the process of decarbonylation, which is 370.8 kJ/mol. Lignin is a process of de-side chaining, and the highest reaction energy barrier also appears in the process of decarbonylation, which is 374.9 kJ/mol. With the temperature further increases, the number of benzene rings further increases. The pathway that naphthalene dehydrogenates to form naphthalene free radicals and then reacts with ethylene twice by addition action, finally cycles and isomerizes to produce phenanthrene is mostly to happy, for the barrier is lowest, that is 38.6 kJ/mol.

Conflicts of Interest: The authors declare that they have no conflicts of interest to report regarding the present study.

References

1. Nada, A., Ahmed, A., Maryam, K., Vega, L. F., Abu-Zahra, M. R. M. (2021). Activated carbons from biomass-based sources for CO_2 capture applications. *Chemosphere, 282,* 131111–131111. DOI 10.1016/j.chemosphere.2021.131111.

2. Jerzy, S. M., Pawel, D., Michal, K., Ewelina, O. (2021). Solid biomass energy potential as a development opportunity for rural communities. *Energies, 14(12),* 3392–3398. DOI 10.3390/EN14123398

3. Guo, F. Q., Zhao, X. M., Peng, K. Y., Liang, S., Jia, X. P. et al. (2019). Catalytic reforming of biomass primary tar from pyrolysis over waste steel slag based catalysts. *International Journal of Hydrogen Energy, 44(31),* 16224–16233. DOI 10.1016/j.ijhydene.2019.04.190.

4. Devi, L., Ptasinski, K. J., Janssen, F. J. J. G., Paasen, S. V. B. V., Bergman, P. C. A. (2005). Catalytic decomposition of biomass tars: Use of dolomite and untreated olivine. *Renewable Energy, 4(30),* 565–587. DOI 10.1016/j.renene.2004.07.014.

5. Milne, T. A., Abatzoglou, N., Evans, R. J. (1998). Biomass gasification "Tars": Their nature, formation and conversion. *NERL Technical Report (NERL/TP-570-25357).*

6. Dayton, D. C. (2002). A Review of the literature on catalytic biomass tar report destruction. *NERL Milestone Completion Report (NERL/TP-510-32815).*

7. Moersch, O., Spliethoff, H., Hein, K. R. G. (2000). Tar quantification with a new online analyzing method. *Biomass and Bioenergy, 18(1),* 79–86. DOI 10.1016/S0961-9534(99)00068-9.

8. Cavalli, A., Aravind, P. V. (2021). Effect of selected representative biomass gasification tar compounds on Ni-GDC solid oxide fuel cells. *International Journal of Hydrogen Energy, 46(40),* 21124–21135. DOI 10.1016/j.ijhydene.2021.03.188.

9. Evans, R. J., Milne, T. A. (1987). Molecular characterization of the pyrolysis of biomass.1.Foudamental. *Energy & Fuels, 1(2),* 123–137. DOI 10.1021/ef00002a001.

10. Elliott, D. C. (1988). *Relation of reaction time and temperature to chemical composition of pyrolysis oils.* Washington: ACS Publications.

11. Hasler, P., Nussbaumer, T. (2000). Sampling and analysis of particles and tars from biomass gasifiers. *Biornass and Bioenergy, 18(1),* 61–66. DOI 10.1016/S0961-9534(99)00071-9.

12. Perez, P., Aznar, P. M., Caballero, M. A., Gil, J., Martin, J. A. et al. (1997). Hot gas cleaning and upgrading with acalcined dolomite located downstream a biomass fluidised bed gasifier operating with steam-oxygen mixtures. *Energy Fuels, 11,* 1194–203. DOI 10.1021/ef970046m.

13. Corella, J., Toledo, J. M., Aznar, M. P. (2002). Improving the modeling of the kinetics of the catalytic tar elimination in biomass gasification. *Industrial and Engineering Chemistry Researchs, 41(14),* 3351–3356. DOI 10.1021/ie0110336.

14. Wang, S. R., Luo, Z. Y. (2013). *Pyrolysis of biomass components.* Beijing: Science Press.

15. Zhang, Z., Liu, C., Li, H. J., Huang, J. B., Huang, X. L. (2011). Theoretical studies of pyrolysis mechanism of xylan monomer. *Acta Chimica Sinica, 69(18),* 2099–2107.

16. Huang, J. B., Liu, Z., Ren, L. R., Tong, H., Li, W. M. et al. (2013). Studies on pyrolysis mechanism of syringol as lignin model compound by quantum chemistry. *Journal of Fuel Chemistry and Technology, 41(6),* 657–661. DOI 10.1016/S1872-5813(13)60031-6.

17. Huang, J. B., Wu, S. B., Lei, M., Cheng, H., Liang, J. J. et al. (2015). Quantum chemistry study on pyrolysis mechanism of lignin dimer model compound. *Journal of Fuel Chemistry and Technology, 43(11),* 1334–1338. DOI 10.3969/j.issn.0253-2409.2015.11.008

18. Yang, H., Wang, J. H., Qiao, C. Z., Xu, Q. L. (2012). Catalytic cracking mechanism of a bio-oil model compound. *Petrochemical Technology, 41(8),* 876–881. DOI 10.3969/j.issn.1000-8144.2012.08.002

19. Xiong, Z., Wang, Y., Syed-Hassen, S. S. A., Hu, X., Han, H. et al. (2018). Effects of heating rate on the evolution of bio-oil during its pyrolysis. *Energy Conversion and Management, 163,* 420–427. DOI 10.1016/j.enconman.2018.02.078.

20. Xiong, Z., Guo, J. H., Chaiwat, W., Hu, X., Han, H. D. et al. (2020). Assessing the chemical composition of heavy components in bio-oils from the pyrolysis of cellulose, hemicellulose and lignin at slow and fast heating rates. *Fuel Processing Technology, 199,* 106299–106299. DOI 10.1016/j.fuproc.2019.106299.

21. Huang, J., Liu, C., Ren, L. (2013). Studies on pyrolysis mechanism of syringol as lignin model compound by quantum chemistry. *Journal of Fuel Chemistry and Technology, 41(6),* 657–661. DOI 10.1016/S1872-5813 (13)60031-6.

22. Li, Y. L., Wu, Z. S. (2009). Effects of catalytic cracking conditions on biomass tar cracking. *Journal of Tsinghua University (Science and Technology), 49(2),* 253–257. DOI 10.16511/j.cnki.qhdxxb.2009.02.005

23. Kislov, V. V., Mebel, A. M., Lin, S. H. (2002). Ab initio and DFT study of the formation mechanisms of polycyclic aromatic hydrocarbons: The phenanthrene synthesis from biphenyl and naphthalene. *Journal of Physical Chemistry A, 106,* 6171–6182. DOI 10.1021/jp020406t.

24. Xiong, Z., Han, H. D., Azis, M. M., Hu, X., Wang, Y. et al. (2019). Formation of the heavy tar during bio-oil pyrolysis: A study based on Fourier transform ion cyclotron resonance mass spectrometry. *Fuel, 239,* 108–116. DOI 10.1016/j.fuel.2018.10.151.

25. Xiong, Z., Syed-Hassen, S. S. A., Hu, X., Guo, J. H., Qiu, J. H. et al. (2019). Pyrolysis of the aromatic-poor and aromatic-rich fractions of bio-oil: Characterization of coke structure and elucidation of coke formation mechanism. *Applied Energy, 239,* 981–990. DOI 10.1016/j.apenergy.2019.01.253.